

*Supporting information for*

# A General Method to Measure Hall Effect in Nanowires: Examples of FeS<sub>2</sub> and MnSi

*John P. DeGrave, Dong Liang, Song Jin\**

Department of Chemistry, University of Wisconsin—Madison 1101 University Avenue,  
Madison, Wisconsin 53706, USA

E-mail: [jjin@chem.wisc.edu](mailto:jjin@chem.wisc.edu)

## **I. Experimental Details for Fabricating Nanowire Hall Effect Devices**

Nanowires (NWs) are deposited onto a Si/SiO<sub>2</sub> (600 nm) substrate either by dry transfer or by drop casting from an ethanol dispersion created by sonicating the growth substrate in 3-4 drops of ethanol for about 10 s. In the case of drop casting, nitrogen gas is flown across the surface of the device substrate which tends to align the NWs with the stream of nitrogen. The substrate covered with aligned NWs is then loaded into a metal deposition system for deposition of insulating alumina (Al<sub>2</sub>O<sub>3</sub>) by e-beam evaporation without tilting the sample stage. The thickness of the alumina layer depends on the NW material as discussed in the main text, typically 40 nm for nanowires of FeS<sub>2</sub> and MnSi.

Next, a numeric grid with alignment marks and wire bonding pads is patterned on the device substrate in the first lithographic step using a Zeiss LEO Supra 55 VP (30 kV) scanning electron

microscope (SEM) and Nanometer Pattern Generation System (NPGS) e-beam system. We implement a MMA/PMMA bilayer e-beam resist (MicroChem) for all e-beam lithography steps and develop the exposed patterns in 1:3 IPA:MIBK solution (MicroChem). For the numeric grid and bonding pads, a metallic bi-layer of 40 nm Ti and 30 nm Au are deposited via e-beam evaporation.

After liftoff in acetone, the positions of the NWs on the numerical grid are located and recorded digitally using a dark-field optical microscope. The lithographic pattern was then designed using NPGS and DesignCAD LT2000 software. The first layer is written via e-beam lithography and the pattern developed, and then the device substrate is subjected to a 30 s, 100 W oxygen plasma etch and 3-5 s buffered HF (Buffered HF improved, Transene Company Inc.) etch prior to metal deposition. The device substrates are loaded onto a sample stage tilted 45° with respect to the incident angle of evaporated material. The first electrode contact layer is then deposited and the choice of contact metal depends upon the necessary conditions for ohmic contact. In the case of FeS<sub>2</sub> nanostructures either Au or Ti/Au is used, and in the case of MnSi NWs a Ti/Au bilayer is used. The total electrode thickness ranged between 60 and 110 nm with no observable difference in device performance. After another round of e-beam lithography to define the second set of opposing electrode pattern, the final contact electrode layer is then deposited with the device substrate flipped the opposite direction but still on the sample stage tilted 45° with respect to the incident angle of evaporated material to allow the contact to the opposite sidewall of the NW device (see schemes in Figure 1a-c of the main text).

## II. Hall Devices without the Insulating $\text{Al}_2\text{O}_3$ Layer

To demonstrate the importance of the insulating alumina layer, we show in Figure S1 the device measurement results for two  $\text{FeS}_2$  Hall devices that were fabricated without the alumina deposition step (but otherwise the same as shown in Figure 1a-c of the main text). The extracted Hall voltage is observed to oscillate about zero, thus the calculated Hall coefficient will also oscillate about zero in stark contrast to devices that include the insulating alumina layer, as presented in the main text.

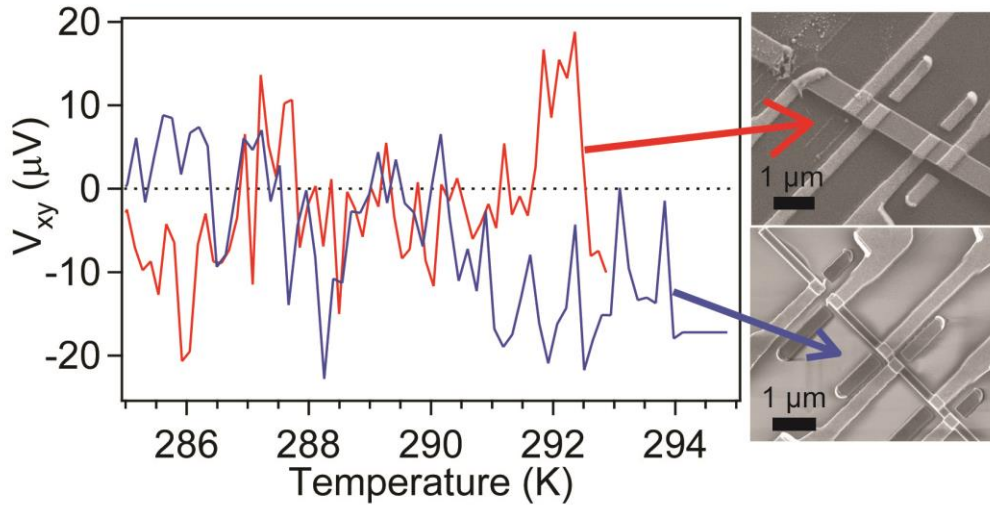


**Figure S1.**  $\text{FeS}_2$  nanowire hall devices without the insulating  $\text{Al}_2\text{O}_3$  layer. The Hall voltage oscillates about zero, clearly demonstrating the importance of including an insulating layer on the top of the nanowire to prevent the Hall voltage from shorting. The SEM images on the right were taken after the devices were measured and broke. The red line corresponds to a  $\text{FeS}_2$  nanobelt device with 550 nm width and the blue line corresponds to a  $\text{FeS}_2$  nanowire device with 220 nm width.

### III. Cylindrical NW Hall Device

The Hall device fabrication and measurement methodology developed in this work is general to other materials and to samples with both circular and square cross-sections. We also used a Si NW with 100 nm diameter to demonstrate the generality of the Hall device fabrication process. Figure S3a and inset show the cross-section and perspective schematics for a finished cylindrical NW device fabricated using the same procedure described in Figure 1a-c in the main text. Figure S3b shows the SEM of a representative finished device using a silicon NW with circular cross-section and the desired device geometry.

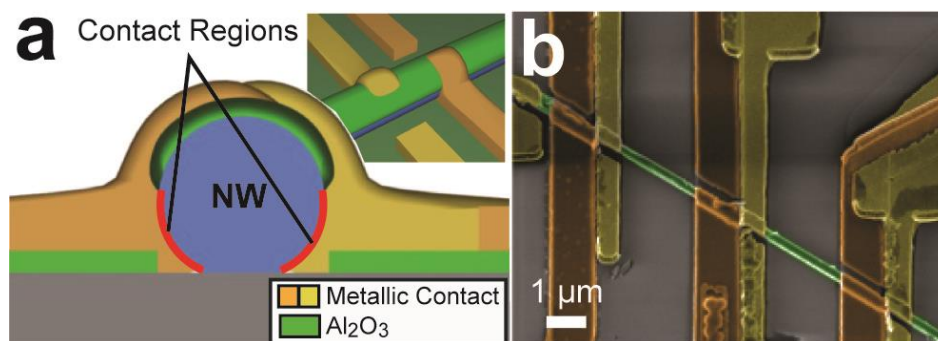


**Figure S2.** a) Schematic cross-section and perspective (inset) views of completed cylindrical Hall NW device. b) False color SEM of final cylindrical NW Hall effect device (fabricated from a 100 nm diameter Si NW for demonstration).

### IV. Additional Hall Device Comparisons

The scattered plots of the Hall coefficient and Hall mobility determined from Hall measurements at 295 K in correlation with various parameters for 23 devices are collected in Figure S2. The Hall coefficient and Hall mobility determined from Hall measurements do not correlate with any geometrical or measurement parameters that might convolute the comparison of different device morphologies (i.e. FeS<sub>2</sub> nanowires versus nanorods and nanoplates).

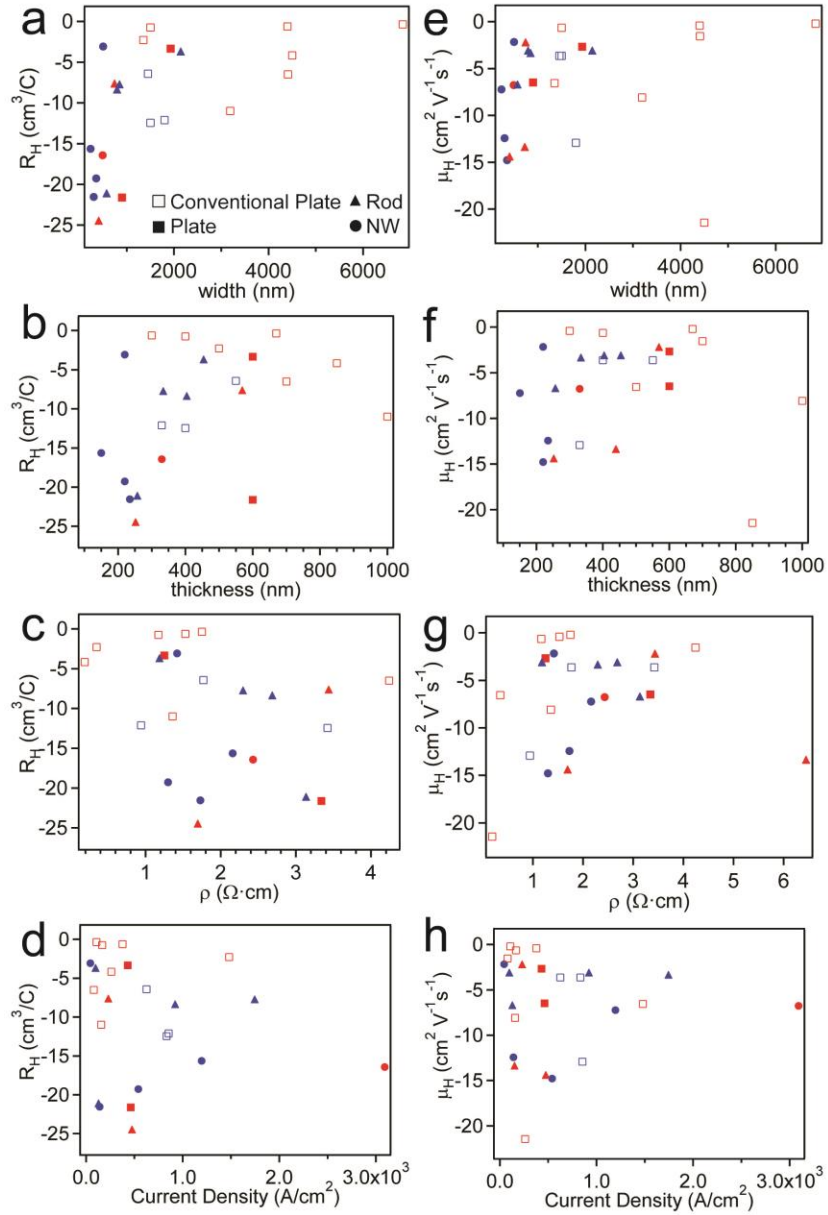


**Figure S3.** Additional data plots for 23 FeS<sub>2</sub> Hall devices showing the (lack of) correlation of Hall coefficient and Hall mobility determined from Hall measurements with various parameters. a-d) The calculated Hall coefficient is plotted versus device width, thickness, resistivity and current density to show the absence of correlation. e-h) The calculated Hall mobility is plotted versus device width, thickness, resistivity and current density to show the absence of correlation.

Blue symbols correspond to 10 devices also presented in Table 1 (main text) and represent the highest quality (low noise) data sets. Red symbols are extracted from 13 additional device sets.

#### IV. Additional MnSi NW Hall Device

An additional MnSi NW device is included here to demonstrate the generality of the qualitative features observed for MnSi NWs. For this particular MnSi NW device, the Hall resistivity is only shown up to 2.0 T, but the “knee” features mentioned in the main text still are clearly seen in the 28 K (purple) and 20 K (red) traces at approximately the same field values.

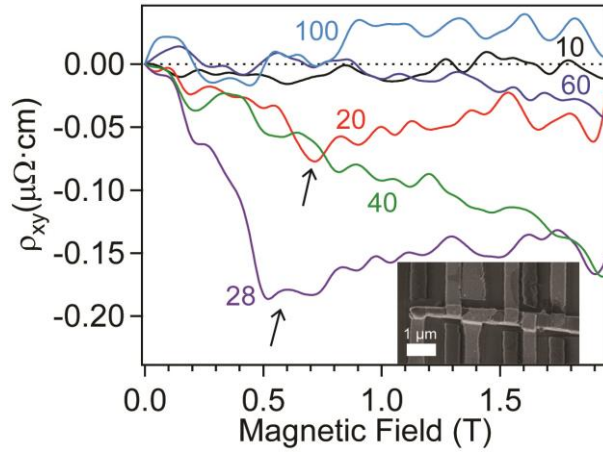


**Figure S4.** Hall resistivity ( $\rho_{xy}$ ) versus applied magnetic field at several temperatures for a MnSi NW Hall device with a rhombohedra cross-section measuring  $420 \text{ nm} \times 240 \text{ nm}$  (SEM image of the finished device shown as inset). Arrows indicate the “knee” feature of the anomalous Hall effect signal.

#### V. Bulk MnSi Hall Resistivity Data

The bulk MnSi Hall resistivity data from Lee et al.<sup>S1</sup> and Neubauer et al.<sup>S2</sup> showing the anomalous Hall effect are reproduced below for comparison to our result for a MnSi NW Hall device (shown in Figure 5 in the main text) to demonstrates qualitatively similar behavior.

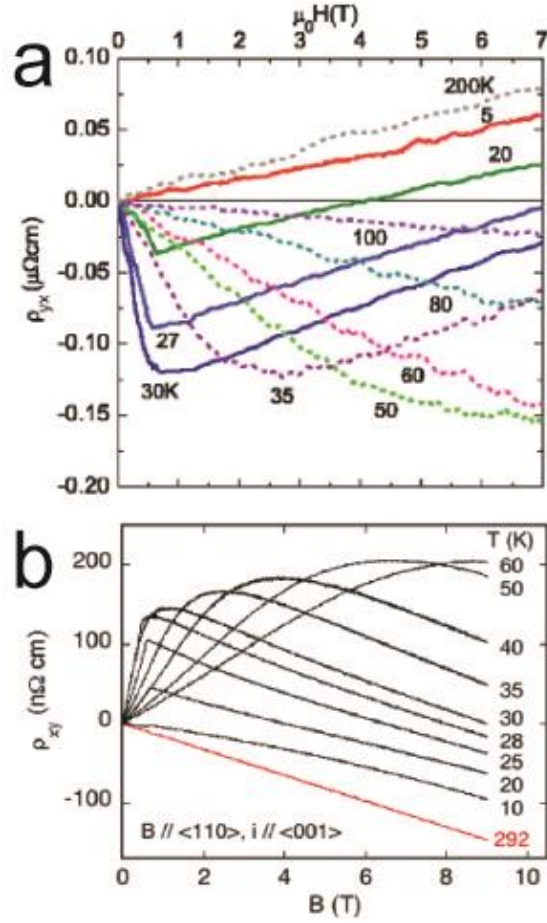


**Figure S5.** Previously reported Hall resistivity for bulk MnSi versus applied magnetic field from

a) Lee et al.<sup>S1</sup> and b) Neubauer et al.<sup>S2</sup>

## References

- S1. Lee, M.; Onose, Y.; Tokura, Y.; Ong, N. P. *Phys. Rev. B* **2007**, *75*, 172403-1/172403-4.  
S2. Neubauer, A.; Pfleiderer, C.; Binz, B.; Rosch, A.; Ritz, R.; Niklowitz, P. G.; Boni, P. *Phys. Rev. Lett.* **2009**, *102*, 186602-1/186602-4.